



# Particle Identification by Pulse-Shape Analysis with Neural Network

Yuto HIJIKATA<sup>1</sup>, Takahiro KAWABATA<sup>2</sup>, Yoshiko KANADA-EN'YO<sup>1</sup>, Kenichi YOSHIDA<sup>1</sup>, Yui ARAKAWA<sup>1</sup>, Kento INABA<sup>1</sup>, Shiyo ENYO<sup>1</sup>, Shintaro OKAMOTO<sup>1</sup>, Kazuki KATAYAMA<sup>1</sup>, Ryota KONGO<sup>1</sup>, Akane SAKAUE<sup>1</sup>, Kosuke SAKANASHI<sup>2</sup>, Shu TAKAGI<sup>1</sup>, Takanobu Doi<sup>1</sup>, Yuki FUJIKAWA<sup>1</sup>, Tatsuya FURUNO<sup>3</sup>, Rinko MATSUMOTO<sup>1</sup>, Takuya MIKAMI<sup>1</sup>, Keiko MIYAZATO<sup>1</sup> and Motoki MURATA<sup>3</sup>

<sup>1</sup>Department of Physics, Kyoto University, Kitashirakawa Oiwake, Sakyo, Kyoto 606-8502, Japan

<sup>2</sup>Department of Physics, Osaka University, 1-1 Machikaneyama, Toyonaka, Osaka 560-0043, Japan

<sup>3</sup>Research Center for Nuclear Physics, Osaka University, 10-1 Mihogaoka, Ibaraki, Osaka 567-0047, Japan

E-mail: [hijikata.yuto.23u@st.kyoto-u.ac.jp](mailto:hijikata.yuto.23u@st.kyoto-u.ac.jp)

(Received September 30, 2019)

We have performed a pulse-shape analysis of signals from Si detectors to identify low-energy charged particles with neural networks (NNs). We acquired pulse shapes of proton, deuteron, triton,  ${}^3\text{He}$  and  ${}^4\text{He}$  from a CH<sub>2</sub> target bombarded by  $\alpha$  particles. We trained the NNs using the pulse shapes for known particles and evaluated their particle-identification ability of the NNs. The NNs successfully distinguished helium isotopes from hydrogen isotopes, but could not separate the helium isotopes into  ${}^4\text{He}$  and  ${}^3\text{He}$ .

**KEYWORDS:** particle identification, pulse shape analysis, neural network, silicon detector

## 1. Introduction

### 1.1 Motivation

Recent cluster-model calculations predict that  $\alpha$  condensed states emerge in self-conjugated  $N = 4n$  nuclei. In the  $\alpha$  condensed states, all of the  $\alpha$  particles are condensed in the lowest-energy orbits, and their matter density is as low as 1/4–1/5 of normal nuclear states [1]. Thus, observation of the  $\alpha$  condensed states is important for clarifying physical properties of the low-density nuclear matter, for example, appearing on the surface of neutron stars.

T. Yamada and P. Schuck calculated energies of the  $\alpha$  condensed states in  $N = 4n$  nuclei and suggested that  $\alpha$  condensed states appear at 1–3 MeV above  $N\alpha$  decay thresholds [2]. The wave functions of the  $\alpha$  condensed states in the  $N = 4n$  nuclei have large overlaps with those in the lighter  $N = 4n$  nuclei. Once the  $\alpha$  condensed states are excited, they are expected to decay by emitting multiple  $\alpha$  particles with energies of 1–3 MeV. Thus, we aim at searching  $\alpha$  condensed states by measuring low-energy  $\alpha$  particles over large solid angles around a target in the inelastic  $\alpha$  scattering.

However, it is not easy to detect and identify such low-energy particles over large solid angles. One of the conventional particle identification (PID) methods is an  $E$ - $\Delta E$  method. In the  $E$ - $\Delta E$  method, a couple of  $\Delta E$  and  $E$  detectors are used. The  $\Delta E$  detector is a thin detector which charged particles penetrate, while the  $E$  detector is a thick detector in which charged particles stop. The charged particles are identified from the correlation between dropping energies at  $\Delta E$  and  $E$  detectors. This is a very reliable method, but cannot be applied to our research because there are currently no large Si detectors which low-energy  $\alpha$  particles with  $E < 3$  MeV can penetrate. Another PID method is a time of flight method, in which PID is performed by using a correlation between flight



time from a target to a detector and the detected energy, but this method can determine mass numbers only. In addition, since it is necessary to keep distance between the detector and the target long enough to achieve good mass resolution, consequently solid angles of the detectors become smaller. Therefore, in order to search for  $\alpha$  condensed states with high sensitivity, it is essential to develop a new PID method for low-energy charged particles over large solid angles.

### 1.2 Pulse-Shape Analysis

In the present study, we have attempted to identify particles by a pulse-shape analysis (PSA). The PSA utilizes a property that the pulse shapes induced by charged particles stopping in Si detectors differ depending on the type of the particles. This technique was studied in many previous researches and established for high-energy ( $>$  about 100 MeV) heavy ions ( $A \geq 12$ ) [3–8], but not enough for low-energy light ions. Particularly, there are no reports that low-energy particles with  $E < 2$  MeV were successfully separated by the PSA.

In the conventional PSA method, PID was performed by defining several parameters that reflect the pulse shapes, and comparing them between different particles. Therefore, multi-dimensional information from the pulse shapes was contracted to the several parameters and some parts of the information were lost. To solve this problem, we tried to introduce a multi-dimensional analysis with neural networks (NNs). The PSA with NNs was performed in a previous research [8], but only high-energy heavy ions were analyzed. Thus, we detected light charged particles with  $E = 1\text{--}3$  MeV by Si detectors and acquired pulse shapes induced by these particles to train NNs. In this paper, we report the experimental details, the construction of the NNs, and their PID ability.

## 2. Experiment

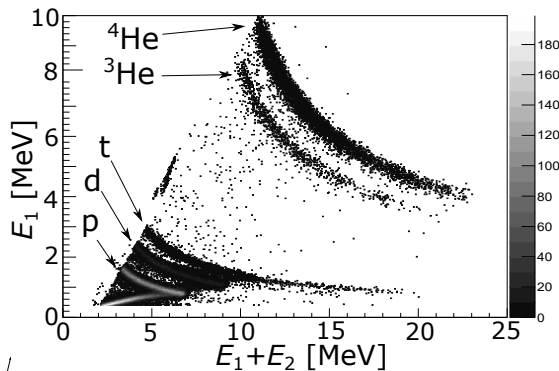
The measurement to acquire pulse shapes was performed at Research Center for Nuclear Physics, Osaka University in July, 2018. A  ${}^4\text{He}$  beam at 87.2 MeV bombarded a  $\text{CH}_2$  target and charged particles (proton, deuteron, triton,  ${}^3\text{He}$ ,  ${}^4\text{He}$ ) emitted from the target were detected by three stacked Si detectors. Signals from the second layer Si detector (325  $\mu\text{m}$  thick, 2304  $\text{mm}^2$  as active area), in which  $\alpha$  particles with energy below 35 MeV stopped, were used for the PSA. The first Si detector (65  $\mu\text{m}$  thick, 2304  $\text{mm}^2$  as active area) was installed as a  $\Delta E$  detector. In other words, we acquired signals for both the  $E\text{-}\Delta E$  method and the PSA at the same time. In the analysis described below, the particle types were determined by the  $E\text{-}\Delta E$  method at first, and the PSA with the NNs was performed for these particles. Additionally, the third Si detector (500  $\mu\text{m}$  thick, 2304  $\text{mm}^2$  as active area) was installed to veto punch through events in which charged particles penetrated the  $E$  detector (the second layer Si detector), because we were interested in particles stopping at the second detectors only.

The Si detectors were connected to the charge-sensitive pre-amplifier and the pulse shapes were acquired by the FADC (CAEN V1730), which recorded 4100 points per event with a sampling rate of 500 MHz. The measured energies were calibrated by using the  ${}^{148}\text{Gd}$ ,  ${}^{241}\text{Am}$ , and  ${}^{244}\text{Cm}$   $\alpha$  sources.

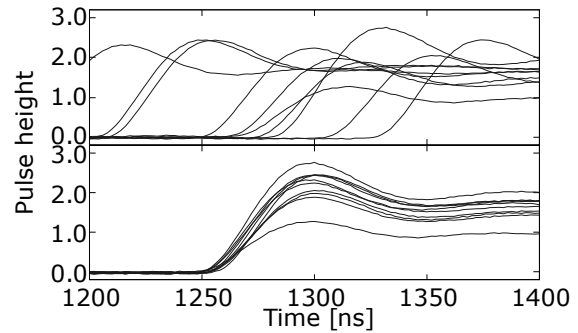
## 3. Making Data Set

Figure 1 shows the correlation between energies measured by the first Si detector ( $E_1$ ) and the sum of  $E_1$  and energies measured by the second Si detector ( $E_2$ ) when charged particles penetrate the first detector. It can be seen that hydrogen isotopes (proton, deuteron, and triton) and helium isotopes ( ${}^3\text{He}$  and  ${}^4\text{He}$ ) are clearly separated.

Then, we selected low-energy particles. Since it is necessary to identify particles with  $E = 1\text{--}3$  MeV for our purpose, we analyzed low-energy particles with  $1 \text{ MeV} < E_2 < 3 \text{ MeV}$  only. Since the number of recorded tritons ( ${}^3\text{He}$ ) was small, we enlarged the energy ranges to  $1 \text{ MeV} < E_2 < 5$  (10)



**Fig. 1.** Correlation between  $E_1$  and the sum of  $E_1$  and  $E_2$ .  $E_1$  and  $E_2$  mean deposited energies at first and second Si detectors.



**Fig. 2.** (a) Typical pulse shapes of the RDS. (b) Typical pulse shapes of the SDS.

MeV when we analyzed these particles.

In this experiment, peak time, namely the time when pulse heights became maximum, differs depending on types and energies of detected particles due to the experimental conditions. So, NNs were likely to be biased by the peak time which could change event by event. To prevent this bias, we prepared two data sets in which the timing information was modified. In the first data set "random data set (RDS)", the peak time of signals was randomly shifted in the step of 2 ns between 1200 and 1400 ns as seen in Fig. 2(a). On the other hand, in the second data set "simultaneous data set (SDS)", the peak time was fixed at 1300 ns as seen in Fig. 2(b). Each event in these data sets contains 3900 points which correspond to 0–7798 ns in units of 2 ns after fixing the peak times. We applied these data sets to the NNs as described in next section.

#### 4. Neural Networks

NNs generally consist of the three kinds of layers, the input layer, the output layer, and the hidden layers which connect between the input and output layers. Various NNs with different structures of hidden layers are available for diverse purposes. In the present work, we selected the convolutional neural network (CNN) for the PSA. The CNN is mainly used for image recognition, but also for analyzing time-series data as in the present case. We used the Keras [9] and Tensorflow [10] libraries to construct the CNN as shown in Fig. 3.

In the present NNs, the two convolution layers find features of input pulse shapes. The following max pooling layer compresses the output information from the convolution layer to enable NNs to identify particles regardless of the peak time. Next, the first fully connected layer (FCL) correlates the features outputted from the pooling layer and determines the important features. Finally, the second FCL transforms outputs from the first FCL into the probability of each particles. Each layer has several parameters which we should tune manually. We adjusted these parameters to maximize PID accuracy by the NNs.

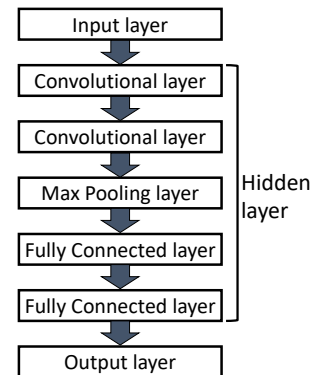


**Fig. 3.** Structure of the present NN.

## 5. Training and Result

We trained four CNNs for discriminating  $\alpha$  particles and other particles (proton, deuteron, triton and  $^3\text{He}$ ) to maximize their PID ability. The accuracy was evaluated by comparing their outputs with the correct answers acquired from the  $E-\Delta E$  method. Even if the NNs can correctly identify other particles used for training, it is not always possible to correctly identify particles not used for training. Thus, we used 80% of the RDS for training and we tested the networks by 20% of the RDS after the training. Additionally, we applied these networks to the SDS. The results are summarized in Table I. Helium and hydrogen were successfully separated with  $\geq 95\%$  accuracy for both of the RDS and SDS. But, He isotopes could not be separated.

**Table I.** Accuracy of PID by the NNs presented with (numbers of successful PID events)/(number of total events).

	p & $\alpha$	d & $\alpha$	t & $\alpha$	$^3\text{He}$ & $\alpha$
Energy range [MeV]	1–3	1–3	1–5	1–10
Train data accuracy	955/960 99.5%	948/960 98.8%	954/960 99.4%	886/1280 69.22%
Test data accuracy	237/240 98.8%	230/240 95.8%	238/240 99.2%	192/320 60.0%
SDS accuracy	1193/1200 99.42%	1171/1200 97.58%	1190/1200 99.17%	

## 6. Summary and Future

We attempted a PSA with NNs in order to discriminate low-energy light particles. We acquired pulse shapes of signals from the Si detector induced by charged particles which were identified by the conventional  $E-\Delta E$  method. These data were used for training and testing the NNs. As a result, the NNs successfully distinguished  $\alpha$  particles from hydrogen isotopes, but hardly separated Helium isotopes into  $^3\text{He}$  and  $^4\text{He}$ .

## References

- [1] T. Yamada and P. Schuck, Eur. Phys. J. A **26**, 185 (2005).
- [2] T. Yamada and P. Schuck, Phys. Rev. C **69**, 024309 (2004).
- [3] C. A. J. Ammerlaan, Nucl. Instrum. Methods **22**, 189 (1963).
- [4] G. Pausch, et al., IEEE Trans. Nucl. Sci. **43**[3], 1097 (1996).
- [5] G. Pausch, et al., IEEE Trans. Nucl. Sci. **44**[3], 1040 (1997).
- [6] H. Hamrita, et al., Nucl. Instrum. Methods Phys. Res. A **531**, 607 (2004).
- [7] S. Barlini, et al., Nucl. Instrum. Methods Phys. Res. A **600**, 644 (2009).
- [8] J.L. Flores, et al., Nucl. Instrum. Methods Phys. Res. A **830**, 287 (2016).
- [9] Keras Documentation (<https://keras.io/ja/>).
- [10] TensorFlow (<https://www.tensorflow.org/>).